

When Surfaces Lie: Exploiting Wrinkle-Induced Attention Shift to Attack Vision-Language Models

Chengyin Hu, Xuemeng Sun, Jiajun Han, Qike Zhang, Xiang Chen, Xin Wang, Yiwei Wei, Jiahua Long

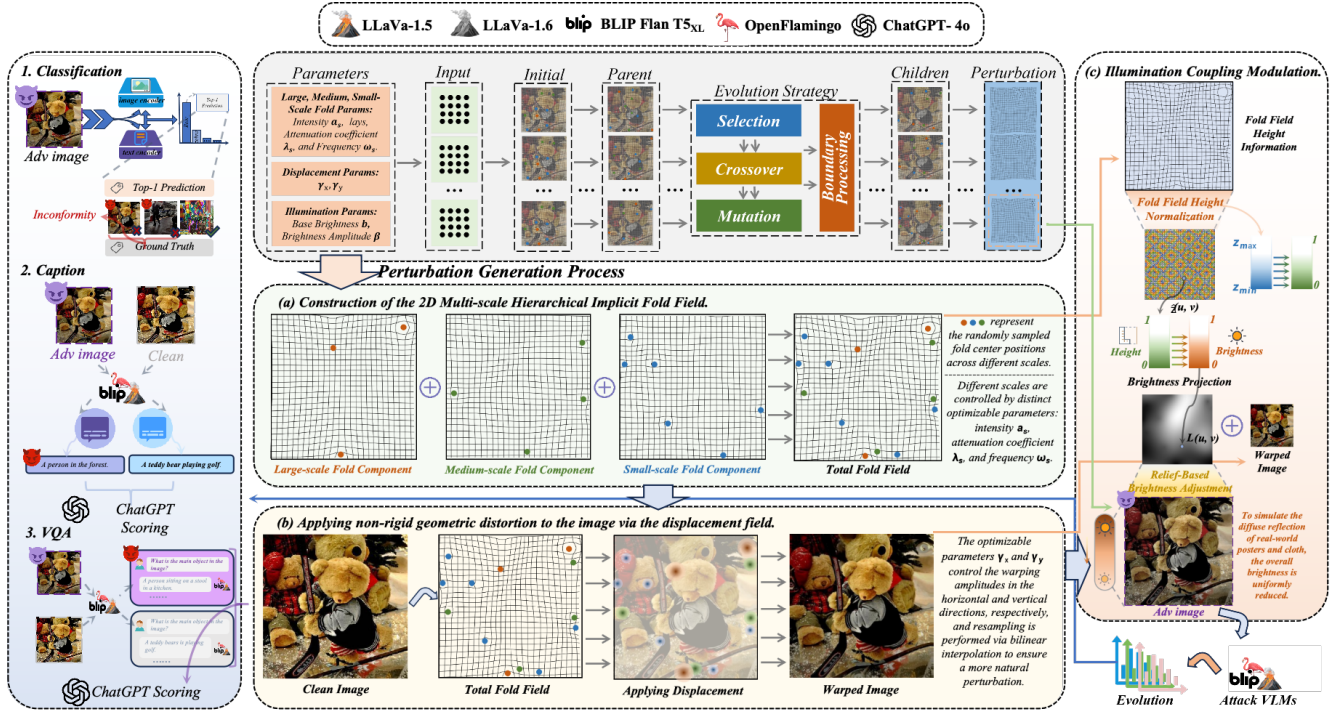


Figure 1: Overview of the Proposed Wrinkle-Based Structural Attack Framework. The framework simulates wrinkle-like non-rigid deformation through multi-scale wrinkle modeling, displacement-field warping, and illumination-coupled modulation, and then optimizes the perturbation parameters with a genetic algorithm to generate adversarial examples for multiple vision-language Tasks.

Abstract

Visual-Language Models (VLMs) have demonstrated exceptional cross-modal understanding across various tasks, including zero-shot classification, image captioning, and visual question answering. However, their robustness to physically plausible non-rigid deformations—such as wrinkles on flexible surfaces—remains poorly understood. In this work, we propose a parametric structural perturbation method inspired by the mechanics of three-dimensional fabric wrinkles. Specifically, our method generates photorealistic non-rigid perturbations by constructing multi-scale wrinkle fields and integrating displacement field distortion with surface-consistent appearance variations. To achieve an optimal balance between visual naturalness and adversarial effectiveness, we design a hierarchical fitness function in a low-dimensional parameter space and employ an optimization-based search strategy. We evaluate our approach using a two-stage framework: perturbations are first optimized on a zero-shot classification proxy task and subsequently assessed for transferability on generative tasks. Experimental results demonstrate that our method significantly degrades the performance of

various state-of-the-art VLMs, consistently outperforming baselines in both image captioning and visual question-answering tasks.

Keywords

Vision-Language Models; Structural Perturbation; Fabric Wrinkles; Visual Naturalness

1 Introduction

Vision-Language Models (VLMs) have become a major paradigm for cross-modal understanding by jointly modeling visual and textual information. With the rapid progress of large-scale vision-language pre-training and multimodal instruction tuning, VLMs have shown strong generalization across zero-shot classification, image captioning, and visual question answering, and are increasingly viewed as a key route toward open-world visual understanding [1, 8, 11, 17, 24]. Meanwhile, recent advances in test-time generalization, adversarial

robustness, and multimodal safety suggest that VLMs are being deployed as increasingly general-purpose systems in complex environments [10, 22, 32, 34]. A careful understanding of their robustness under practically grounded distortions is therefore essential.

However, existing adversarial studies on VLMs still focus mainly on additive pixel-space perturbations, patch attacks, backdoor attacks, and joint image-text manipulations [7, 33, 37]. Comparatively less attention has been paid to non-rigid structural perturbations that arise in realistic imaging conditions. In practice, inputs may be affected by paper creases, surface irregularities, local shadows, lighting changes, and perspective shifts, especially on approximately diffuse surfaces such as paper, posters, cloth, and recaptured screens. Prior work has shown that non-additive factors, including natural shadows, reflected light, illumination variation, physical-world transformations, and differentiable deformation, can also mislead visual models [3, 12, 14, 21, 23, 25, 28, 36]. Compared with additive perturbations, structure-aware distortions may reorganize contours, textures, and spatial semantic cues in a qualitatively different way, thereby interfering with cross-modal alignment [6]. This raises a central question: can wrinkle-like non-rigid structural distortions expose vulnerabilities of VLMs that are not fully revealed by conventional additive or illumination-dominated attacks?

To answer this question, we propose a parametric perturbation framework centered on wrinkle-like distortion. Instead of explicitly simulating complex three-dimensional surface dynamics, our method defines an implicit multi-scale wrinkle field on the image plane to parameterize surface undulations compactly. A displacement field is then derived to impose non-rigid geometric distortion together with mild surface-consistent appearance variation. In this way, the perturbation is modeled primarily as a structured deformation process rather than a direct pixel-space modification, providing a compact approximation to wrinkle-like imaging distortions in practical scenarios. Because the perturbation is controlled by low-dimensional variables, including wrinkle intensity, layer number, attenuation coefficient, frequency, displacement amplitude, and related appearance parameters, the attack can be formulated as a black-box optimization problem in parameter space. To balance attack effectiveness and visual plausibility, we further design a hierarchical fitness function and employ a genetic algorithm [2, 13] to search for effective perturbation parameters.

Our goal is to examine whether wrinkle-like structural distortion constitutes a distinct and practically meaningful robustness setting for multimodal systems, rather than merely introducing another perturbation type for VLMs. Such perturbations locally reorganize spatial layout rather than merely altering pixel values, and may therefore affect object boundaries, local semantic evidence, and image-text alignment simultaneously. We evaluate the proposed perturbation on zero-shot classification across multiple CLIP models, and then transfer the adversarial examples generated in this surrogate stage to image captioning and visual question answering. Through this unified pipeline, we systematically study the vulnerability of VLMs under wrinkle-like structural perturbations with mild surface-consistent appearance variation. The main contributions of this paper are as follows:

- We propose a wrinkle-like structural attack for VLMs based on multi-scale wrinkle modeling, displacement-field warping, and surface-consistent appearance modulation.
- We conduct extensive experiments on zero-shot classification, image captioning, and visual question answering, showing consistent performance degradation across multiple state-of-the-art vision-language models and stronger attack effectiveness than representative baselines.
- We perform ablation studies on search hyperparameters, multi-scale design, and perceptual weighting, revealing multi-scale complementarity and the trade-off between adversarial effectiveness and visual naturalness.

2 Related Work

2.1 Adversarial Vulnerabilities in VLMs

With the rapid development of vision-language pre-trained Models and large-scale multimodal models, their security in open-world scenarios has attracted increasing attention [33, 37]. Existing studies show that visual-side adversarial perturbations can substantially degrade VLM performance on image classification, image captioning, and visual question answering, and may further affect textual outputs through cross-modal alignment [10]. Subsequent work has investigated transferable attacks against vision-language pre-training models, showing that cross-modal systems can still be misled without access to target-model gradients [22]. More recent studies further extend this line to stronger and sequential transfer attacks, suggesting that VLM vulnerabilities are not limited to a single task but can generalize across multiple downstream settings [30].

2.2 Structured and Physical Perturbations

Compared with pixel-level additive perturbations, structured and physically plausible adversarial disturbances better resemble practical imaging conditions and therefore have greater real-world relevance [7]. Previous studies have shown that natural shadow, reflected light, illumination variation, and deformation can all mislead visual models [14, 21, 23, 25, 28, 36]. For approximately diffuse surfaces, classical reflectance analysis further suggests that changes in surface orientation may induce systematic luminance variation under illumination, providing a physical basis for mild appearance changes associated with wrinkle deformation [5]. These findings indicate that effective real-world attacks need not appear as obvious noise, but may instead manifest as structural distortion, illumination change, or surface undulation. However, existing studies mainly emphasize shadow, lighting, or deformation-based perturbations, while wrinkle-like non-rigid distortions remain largely unexplored in current VLM robustness research [14, 21, 23, 25, 36].

3 Methodology

Figure 1 illustrates the overall framework of the proposed method. We first model wrinkle-like structural perturbations with a multi-scale fold field, convert them into non-rigid geometric warping, and apply a mild appearance adjustment to obtain the final adversarial examples. The perturbation parameters are optimized in a low-dimensional black-box space using a genetic algorithm. The

resulting adversarial examples are evaluated on zero-shot classification and further transferred to image captioning and VQA tasks.

3.1 Problem Definition

This section introduces the proposed wrinkle-like structural perturbation method. Our objective is to assess the robustness of vision-language models under practically motivated structural distortions. Given an input image $x \in \mathbb{R}^{H \times W \times C}$ and its ground-truth label y , we aim to generate a perturbed image x' that changes the model prediction while preserving visual plausibility as much as possible.

In our experiments, the perturbation generation process is modeled as a stochastic parameterized mapping:

$$x' = T_\theta(x; \xi), \quad (1)$$

where θ denotes the perturbation parameters to be optimized, mainly including the intensity, number of layers, decay rate, frequency, displacement magnitude, and related appearance parameters of wrinkles at different scales; ξ denotes the random variables involved in perturbation generation, corresponding to the random sampling of wrinkle center locations at each scale. Since paper bending, surface undulation, and local distortion in practical scenes usually exhibit a certain degree of randomness, we model the perturbation as a stochastic parameterized non-rigid structural perturbation.

For each zero-shot classification model, we adopt an un-targeted attack setting. Let $f: \mathbb{R}^{H \times W \times C} \rightarrow \mathbb{R}^K$ denote the classifier, and let:

$$\hat{y}(x') = \arg \max_{c \in \{1, \dots, K\}} f_c(x'). \quad (2)$$

where $f_c(x')$ denotes the logit (or confidence score) of class c . The attack objective is to find a perturbed image $x' = T_\theta(x; \xi)$ such that:

$$\hat{y}(x') \neq y. \quad (3)$$

The perturbation parameters are optimized independently for each zero-shot classification model. The adversarial examples generated in this stage are then transferred to image captioning and visual question answering to evaluate the cross-task transferability of this type of structural perturbation on generative vision-language tasks.

3.2 Multi-Scale Wrinkle-Like Distortion

To efficiently simulate wrinkle-like non-rigid deformation, we model surface undulation on the image plane with an implicit multi-scale height field.

Let the normalized image coordinates be (u, v) . The total wrinkle field is defined as:

$$z(u, v) = z_L(u, v) + z_M(u, v) + z_S(u, v). \quad (4)$$

Here, $z_L(u, v)$, $z_M(u, v)$, and $z_S(u, v)$ denote the large-scale, medium-scale, and small-scale wrinkle components, respectively. The large-scale component captures the overall bending trend, the medium-scale component describes local hierarchical variation, and the small-scale component supplements fine-grained surface details.

For any scale $s \in \{L, M, S\}$, the corresponding wrinkle component is constructed by superposing multiple local wrinkle sources:

$$z_s(u, v) = \sum_{k=1}^{K_s} a_s \cdot \phi_s(d_{s,k}(u, v)) \cdot \exp(-\lambda_s \cdot d_{s,k}(u, v)), \quad (5)$$

where K_s is the number of wrinkle layers at scale s , a_s is the wrinkle intensity, λ_s is the decay coefficient, and $d_{s,k}(u, v)$ is the distance from position (u, v) to the k -th wrinkle center:

$$d_{s,k}(u, v) = \sqrt{(u - c_{s,k}^u)^2 + (v - c_{s,k}^v)^2}, \quad (6)$$

where $(c_{s,k}^u, c_{s,k}^v)$ denotes the randomly sampled center of the corresponding wrinkle source. Since the spatial distributions of wrinkle centers differ across scales, the resulting field can represent both the overall deformation trend and local structural complexity.

In implementation, different oscillation functions are used at different scales. The large-scale and small-scale components are modeled with sine functions:

$$\phi_L(d) = \sin(\omega_L \pi d), \quad \phi_S(d) = \sin(\omega_S \pi d), \quad (7)$$

while the medium-scale component uses a combination of sine and cosine functions to enrich mid-level structural variation:

$$\phi_M(d) = \frac{1}{2} [\sin(\omega_{M1} \pi d) + \cos(\omega_{M2} \pi d)]. \quad (8)$$

This formulation gives the wrinkle field clear multi-scale hierarchical characteristics. Compared with directly adding independent perturbations in pixel space, it provides a more structured approximation to surface bending, cloth undulation, and local non-rigid deformation in practical scenes.

Displacement field construction and image warping. After generating the wrinkle field $z(u, v)$, we construct a two-dimensional displacement field from its local variations. Intuitively, regions with stronger wrinkle variation should induce stronger stretching, compression, or bending in the corresponding image content. Following common practices in spatial transformation and deformation modeling [15, 25], the displacement field is approximated as:

$$r_u(u, v) = \gamma_u \cdot \frac{\partial z(u, v)}{\partial u}, \quad r_v(u, v) = \gamma_v \cdot \frac{\partial z(u, v)}{\partial v}, \quad (9)$$

where γ_u and γ_v control the distortion magnitudes in the horizontal and vertical directions, respectively. The position with coordinates (u, v) in the original image is then mapped to a new sampling position:

$$\hat{u} = u + r_u(u, v), \quad \hat{v} = v + r_v(u, v). \quad (10)$$

The original image is then resampled by bilinear interpolation to obtain the geometrically distorted image:

$$x_w = W(x, r_u, r_v), \quad (11)$$

where $W(\cdot)$ denotes the image resampling operator based on the displacement field. Rather than modifying colors pixel by pixel, this process reorganizes the spatial layout of image content according to the wrinkle field, producing non-rigid deformation in contours, local structures, and fine-scale details. Compared with additive perturbations, this distortion pattern is more consistent with imaging variations caused by paper bending, surface undulation, or cloth wrinkles in practical scenarios.

Surface-consistent appearance adjustment. In practical scenes, surface undulations may induce mild brightness variation in addition to local geometric changes. To account for this effect, we introduce a lightweight appearance adjustment module after geometric distortion, inspired by illumination-related adversarial perturbations and physical rendering variation [14, 21]. Specifically, image

brightness is adjusted according to the wrinkle field distribution. The wrinkle field is normalized as:

$$\hat{z}(u, v) = \frac{z(u, v) - z_{\min}}{z_{\max} - z_{\min} + \epsilon_z} \quad (12)$$

where z_{\min} and z_{\max} denote the minimum and maximum values of the current wrinkle field, respectively, and ϵ_z is a small constant to prevent division by zero. The brightness modulation map is then constructed as:

$$L(u, v) = b + \beta \cdot \hat{z}(u, v), \quad (13)$$

where b denotes the base brightness and β denotes the amplitude of brightness variation. The final perturbed image is expressed as:

$$x' = \Pi_{[0,1]}(x_w \odot L), \quad (14)$$

where \odot denotes element-wise multiplication, and $\Pi_{[0,1]}(\cdot)$ denotes projecting the input element-wise onto the interval $[0, 1]$ so that the output pixel values remain within the valid range. Under this formulation, the final perturbation is modeled primarily as wrinkle-like structural deformation with mild surface-consistent appearance variation, rather than as a standalone illumination attack.

Perceptual similarity constraint. To balance attack effectiveness and visual plausibility, we introduce a perceptual similarity constraint to measure the visual closeness between the perturbed image and the original image. Since a single metric can hardly capture both structural preservation and high-level perceptual consistency, we combine SSIM [29] and LPIPS [35] to construct a composite perceptual similarity metric:

$$S_{\text{perc}}(x, x') = 0.7 \cdot (1 - S_{\text{LPIPS}}(x, x')) + 0.3 \cdot S_{\text{SSIM}}(x, x'). \quad (15)$$

Here, S_{SSIM} reflects local structural preservation, while S_{LPIPS} measures perceptual distance in a high-level feature space. To make it consistent with SSIM in the optimization objective, we use $1 - S_{\text{LPIPS}}(x, x')$ as a similarity-oriented term within S_{perc} . Their combination jointly constrains structural preservation and perceptual fidelity, thereby encouraging visually plausible perturbations.

Fitness function. For each zero-shot classification model, we define the attack objective as reducing the model's prediction confidence for the true class. Let the predicted probability of the perturbed image x' on the true class y be $p(y | x')$. Then, the adversarial score is defined as:

$$S_{\text{adv}}(x') = -\log(p(y | x') + \epsilon_{\text{adv}}), \quad (16)$$

where ϵ_{adv} is a numerical stability term. For unified modeling with the perceptual similarity term, the attack score is further normalized and denoted as $S_{\text{ladv}} \in [0, 1]$.

On this basis, we adopt a hierarchical fitness design that explicitly prioritizes attack success. First, the attack success indicator is defined as:

$$I(x') = \begin{cases} 1, & \hat{y}(x') \neq y, \\ 0, & \hat{y}(x') = y. \end{cases} \quad (17)$$

$I(x')$ selects the branch of the hierarchical fitness. When the perturbation has not yet caused misclassification, both attack effectiveness and perceptual quality are considered, and the fitness is defined as:

$$F(\theta, \xi) = (1 - \alpha)S_{\text{ladv}} + \alpha S_{\text{perc}}, \quad (18)$$

where $\alpha \in [0, 1]$ balances attack effectiveness and perceptual quality. When the perturbation has already changed the model prediction, the fitness further favors candidates with higher perceptual

quality among successful samples, and is defined as:

$$F(\theta, \xi) = 1 + \eta S_{\text{perc}}, \quad (19)$$

where $\eta \in [0, 1]$ controls the preference for perceptual quality among successful samples.

During the search, attack success is treated as the primary objective, after which the perceptual quality of the perturbed image is further optimized. Since both S_{ladv} and S_{perc} are normalized to $[0, 1]$, the fitness values of unsuccessful samples lie in $[0, 1]$, whereas those of successful samples are greater than 1, thereby explicitly separating successful and failed candidates. This design avoids overly large empirical constants and is more consistent with fitness modeling in genetic algorithms under black-box optimization.

3.3 Genetic Algorithm Optimization

Algorithm 1 Pseudocode of Our Method

Input: original image x , true label y , zero-shot classification model f , parameter space Θ , population size N , maximum generations G , elite size E , mutation rate p_m , stagnation threshold K

Output: optimal perturbation parameters θ^* , perturbed image x'^*

```

1: for  $t = 0$  to  $G - 1$  do
2:   for each  $\theta_i^{(t)} \in P^{(t)}$  do
3:      $x'_i \leftarrow T_{\theta_i^{(t)}}(x; \xi_i)$ 
4:      $S_{\text{adv},i} \leftarrow S_{\text{adv}}(x'_i)$ 
5:      $S_{\text{perc},i} \leftarrow S_{\text{perc}}(x, x'_i)$ 
6:      $F_i^{(t)} \leftarrow F(\theta_i^{(t)}, \xi_i)$ 
7:   end for
8:    $P_{\text{elite}}^{(t)} \leftarrow \text{TopE}(P^{(t)}, F^{(t)})$ 
9:    $Q^{(t)} \leftarrow \text{Select}(P^{(t)}, F^{(t)})$ 
10:   $\tilde{P}^{(t)} \leftarrow C(Q^{(t)})$ 
11:   $\hat{P}^{(t)} \leftarrow M(\tilde{P}^{(t)}, p_m)$ 
12:   $P_{\text{rand}}^{(t)} \sim U(\Theta)$ 
13:   $P^{(t+1)} \leftarrow P_{\text{elite}}^{(t)} \cup \hat{P}^{(t)} \cup P_{\text{rand}}^{(t)}$ 
14:  if stagnation for  $K$  generations then
15:    partially reinitialize  $P^{(t+1)} \setminus P_{\text{elite}}^{(t)}$ 
16:  end if
17: end for
18:  $\theta^* \leftarrow \arg \max_{\theta_i^{(t)}} F_i^{(t)}$ 
19:  $x'^* \leftarrow T_{\theta^*}(x; \xi^*)$ 
20: return  $\theta^*, x'^*$ 

```

Since perturbation generation involves random wrinkle center sampling, geometric resampling, and mild appearance adjustment, the resulting objective is non-convex, nonlinear, and stochastic, making stable optimization difficult for traditional gradient-based methods. Moreover, we consider a black-box attack setting and do not rely on gradient information from the target model. Therefore, a Genetic Algorithm (GA) [13] is adopted to search in the low-dimensional parameter space. The pseudocode of the proposed method is given in Algorithm 1. The method takes the original image, the ground-truth label, the zero-shot classification surrogate model, and the genetic search parameters as inputs, and outputs the optimal perturbation parameters together with the corresponding adversarial example.

Table 1: Performance of VLMs on Zero-shot Classification under Wrinkle-like Structural Perturbations Generated from the COCO Dataset. We report both classification accuracy (ACC) and GPT-4o-based visual naturalness scores. Lower ACC indicates stronger attack effectiveness, while higher GPT-4o scores indicate better visual naturalness. The best results are shown in bold, and the second-best results are underlined.

Method	OpenCLIP ViT-B/16		Meta-CLIP ViT-L/14		EVA-CLIP ViT-G/14		OpenAI CLIP ViT-L/14	
	ACC (%)	GPT-4o	ACC (%)	GPT-4o	ACC (%)	GPT-4o	ACC (%)	GPT-4o
Clean	97	3.65	98	3.65	98	3.65	93	3.65
Natural Light Attack [14]	94 (↓ 3)	<u>2.32</u> (↓ 1.33)	97 (↓ 1)	2.14 (↓ 1.51)	97 (↓ 1)	2.16 (↓ 1.49)	93 (–)	2.07 (↓ 1.58)
Shadow Attack [36]	84 (↓ 13)	2.11 (↓ 1.54)	82 (↓ 16)	1.91 (↓ 1.74)	95 (↓ 3)	2.03 (↓ 1.62)	79 (↓ 14)	1.78 (↓ 1.87)
ITA [21]	<u>46</u> (↓ 51)	2.11 (↓ 1.54)	<u>64</u> (↓ 34)	2.15 (↓ 1.50)	84 (↓ 14)	2.17 (↓ 1.48)	<u>51</u> (↓ 42)	2.15 (↓ 1.50)
Ours (random)	52 (↓ 45)	2.71 (↓ 0.94)	68 (↓ 30)	2.47 (↓ 1.18)	<u>75</u> (↓ 23)	2.89 (↓ 0.76)	53 (↓ 40)	2.64 (↓ 1.01)
Ours (best)	43 (↓ 54)	2.29 (↓ 1.36)	58 (↓ 40)	<u>2.39</u> (↓ 1.26)	66 (↓ 32)	<u>2.72</u> (↓ 0.93)	42 (↓ 51)	<u>2.51</u> (↓ 1.14)

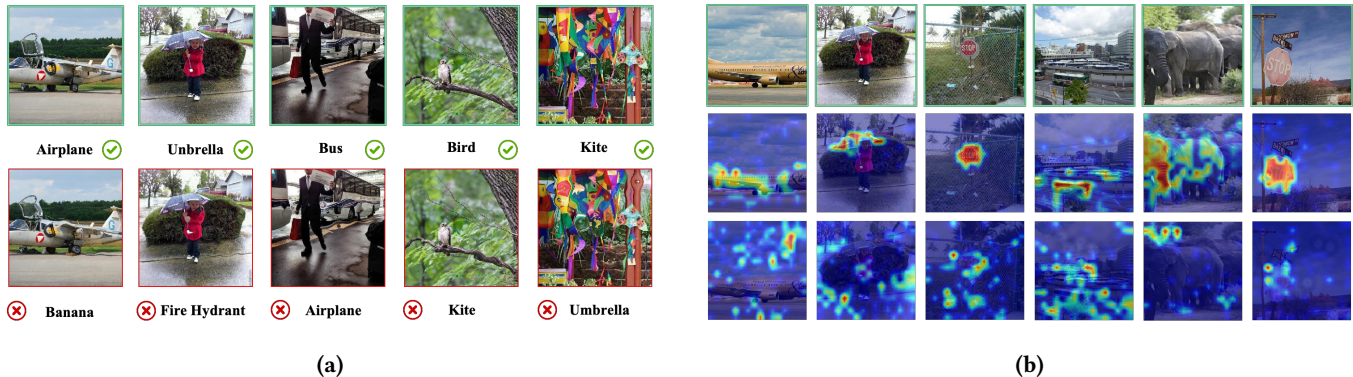


Figure 2: Qualitative Comparison Between Clean and Adversarial Examples. (a) Representative clean and adversarial image pairs, where the proposed perturbation remains visually subtle but causes erroneous predictions on adversarial samples. (b) Comparison of attention visualizations between clean and adversarial images, showing that the perturbation redirects model attention away from semantically meaningful regions.

4 Experiments

4.1 Experimental Setup

To evaluate the proposed wrinkle-like structural perturbation, we conduct experiments on zero-shot classification, image captioning, and visual question answering. In zero-shot classification, four CLIP-based models are independently used to generate and optimize perturbations under the same black-box setting. The adversarial examples are then transferred to image captioning and visual question answering to evaluate cross-task transferability.

Dataset. To ensure consistent comparison across the three tasks, all experiments are conducted on a unified data source, reducing the influence of cross-dataset distribution differences. Specifically, we select 30 categories with 10 images per category from the COCO dataset [18], resulting in 300 clean instance images. For comparison, we follow the same COCO-based evaluation setting as the reference study to keep the data source aligned with the reported baselines [21].

Model Settings. For zero-shot classification, we adopt four CLIP-based models with different visual encoders, including OpenCLIP

ViT-B/16 [8], Meta-CLIP ViT-L/14 [9, 31], EVA-CLIP ViT-G/14 [26], and OpenAI CLIP ViT-L/14 [24]. For image captioning and visual question answering, we use generative vision-language models for transfer evaluation, including LLaVA-1.5 [20], LLaVA-1.6 [19], OpenFlamingo [4], Blip-2 ViT-L [17], Blip-2 FlanT5-XL [16], and InstructBLIP [11]. The baseline methods include Shadow Attack [36], Natural Light Attack [14], and ITA [21]. All methods are evaluated under the same protocol for fair comparison.

Evaluation Metrics. For zero-shot classification, classification accuracy (ACC) is used as the primary metric in the main comparison, while attack success rate (ASR) is additionally reported in the ablation study to reflect search effectiveness. Here, ACC denotes the classification accuracy on the perturbed test set, and ASR denotes the proportion of samples whose predicted labels are altered by the perturbation. We further report a GPT-4o-based visual naturalness score to evaluate the perceptual realism of perturbed images in zero-shot classification. Higher GPT-4o scores indicate better visual naturalness, and all methods are evaluated under the same scoring prompt and protocol. For image captioning, we adopt a judge-based

evaluation protocol and use GPT-4 to assess the semantic consistency between generated captions and image content. For visual question answering, the generated answer and the ground-truth answer are jointly provided to GPT-4, which determines whether the predicted answer is correct. This protocol follows recent robustness studies on large multimodal models and is adopted here to ensure fair comparison under a shared setting [10, 21, 27]. For fair comparison with prior baselines, we follow the reference study in both the COCO-based data setting and the GPT-based evaluation protocol.

Experimental Parameters. In our experiments, wrinkle-like perturbations are searched in a low-dimensional parameter space using a genetic algorithm under a black-box setting. The population size is set to 8, the maximum number of fitness evaluations for each image is set to 350 as the evaluation budget, and the perceptual weighting coefficient α in Eq. (18) is set to 0.3. The perturbation parameters include wrinkle-field generation parameters, displacement parameters, and related appearance parameters. Specifically, the strength ranges of the large- and medium-scale wrinkle components are set to [0.4, 0.8], while that of the small-scale component is set to [0.3, 0.5]; the layer numbers of the large-, medium-, and small-scale components are set to [2, 4], [4, 6], and [6, 8], respectively. The decay and frequency parameters are searched within preset ranges for different scales. The displacement parameters γ_u and γ_v are both set to [0.4, 0.6], while the base brightness and brightness amplitude are set to [0.4, 0.8] and [0.2, 0.4], respectively. In the generative tasks, image captioning and visual question answering directly use the adversarial examples generated in the zero-shot classification stage for transfer evaluation. All experiments are conducted on an RTX 5090 GPU.

4.2 Comparative Experiments

Zero-shot Classification Experiments. We first evaluate the proposed wrinkle-like structural perturbation on zero-shot classification to examine whether it can effectively degrade the recognition performance of CLIP models. For each CLIP model, perturbation parameters are independently optimized using the genetic algorithm, and the resulting adversarial examples are evaluated on the same source model.

As shown in Table 1, the proposed method achieves the strongest attack performance across all four CLIP models in terms of classification accuracy. Compared with clean samples, *Ours (best)* reduces the accuracy of OpenCLIP ViT-B/16, Meta-CLIP ViT-L/14, EVA-CLIP ViT-G/14, and OpenAI CLIP ViT-L/14 by 54, 40, 32, and 51 percentage points, respectively, consistently outperforming Natural Light Attack [14], Shadow Attack [36], and ITA [21]. Meanwhile, *Ours (random)* achieves the highest GPT-4o visual naturalness scores on all four models, indicating that the proposed perturbation can better preserve perceptual realism while maintaining substantial attack effectiveness. These results indicate that the proposed perturbation achieves a favorable trade-off between attack strength and visual naturalness.

Figure 2 (a) presents representative adversarial examples generated by the proposed method. Although the perturbations remain visually subtle and structurally coherent, they are sufficient to induce misclassification. Figure 2 (b) further shows the corresponding

attention visualizations under different CLIP models. Compared with clean images, the perturbed images shift model attention away from semantically relevant object regions toward less informative local textures or surrounding areas. This observation is consistent with the classification degradation, suggesting that the proposed perturbation influences both the final prediction and the intermediate attention distribution.

Evaluation on the Image Captioning Task. We transfer the adversarial examples generated in the zero-shot classification stage to the image captioning task to evaluate the cross-task transferability of the proposed wrinkle-like structural perturbation. As shown in Table 2, *Ours (best)* achieves the lowest semantic consistency scores on all evaluated models, indicating the strongest transfer attack effect among the compared methods. The scores drop to 54.51, 53.15, 30.18, and 58.21 on LLaVA-1.5, LLaVA-1.6, OpenFlamingo, and Blip-2 (FlanT5_{XL}, ViT-L), respectively, for perturbations generated from OpenAI CLIP ViT-L/14, and to 57.08 and 56.57 on Blip-2 (FlanT5_{XL}) and InstructBLIP (FlanT5_{XL}), respectively, for perturbations generated from EVA-CLIP ViT-G/14. Compared with Natural Light Attack [14], Shadow Attack [36], and ITA [21], these results show that the proposed perturbation more effectively disrupts the alignment between visual content and generated descriptions.

This tendency is also reflected in Figure 3 (A). For clean images, the models generally describe the main scene correctly, such as a fighter jet on a runway, a man walking past buses, an empty street with a traffic light, or a bedroom with a bed and a lamp. After perturbation, the generated captions become misleading, often introducing non-existent objects or distorted scene semantics, such as a parked car in the fighter-jet image, a guitar in the bus scene, several cars on the empty road, or two apples in the bedroom scene.

Evaluation on the VQA Task. We further evaluate the generated adversarial examples on the visual question answering task. As reported in Table 3, *Ours (best)* again obtains the lowest answer correctness scores on the evaluated models, indicating a consistently stronger transfer attack effect than Natural Light Attack [14], Shadow Attack [36], and ITA [21]. This further demonstrates effective transfer to downstream VQA reasoning. The correctness scores drop to 45.00, 40.00, 14.00, and 32.00 on LLaVA-1.5, LLaVA-1.6, OpenFlamingo, and Blip-2 (FlanT5_{XL}, ViT-L), for perturbations generated from OpenAI CLIP ViT-L/14, and to 28.00 and 41.00 on Blip-2 (FlanT5_{XL}) and InstructBLIP (FlanT5_{XL}), respectively, for perturbations generated from EVA-CLIP ViT-G/14. Since VQA requires explicit reasoning, the substantial degradation suggests that the proposed perturbation interferes with both visual recognition and fine-grained cross-modal reasoning.

This effect is also evident in Figure 3 (B). For clean images, the models usually answer the questions correctly, such as recognizing that the fighter-jet engines are not started, counting three animals in the scene, or identifying that the dog is lying on a white carpet. After perturbation, the answers become incorrect or semantically inconsistent with the image, for example claiming that the engines are started, undercounting the animals as two, or responding that the object is not a dog. Together with the quantitative results, these examples show that the proposed perturbation effectively disrupts semantic reasoning in downstream VQA systems.

Table 2: Performance Degradation (↓) of VLMs on Image Captioning under Wrinkle-like Structural Perturbations Generated from the COCO Dataset. We compare the semantic consistency scores (%) evaluated by GPT-4 for baseline methods and the proposed method. Lower values indicate stronger attack performance. Numbers in bold denote the best results, and underlined numbers denote the second-best results.

Image Encoder	Models	Params	Clean	Natural Light Attack [14]	Shadow Attack [36]	ITA [21]	Ours (random)	Ours (best)
OpenAI CLIP ViT-L/14	LLaVA-1.5	7B	78.60	77.00 (↓ 1.63)	74.60 (↓ 4.00)	63.73 (↓ 14.87)	56.58 (↓ 22.02)	54.51 (↓ 24.09)
	LLaVA-1.6	7B	72.10	71.70 (↓ 0.39)	71.17 (↓ 0.93)	61.60 (↓ 10.51)	54.45 (↓ 17.65)	53.15 (↓ 18.95)
	OpenFlamingo	3B	70.20	69.53 (↓ 0.67)	67.80 (↓ 2.40)	53.93 (↓ 16.27)	33.59 (↓ 36.61)	30.18 (↓ 50.02)
	Blip-2 (FlanT5XL, ViT-L)	3.4B	75.10	70.77 (↓ 4.33)	68.57 (↓ 6.53)	<u>60.93</u> (↓ 14.27)	61.01 (↓ 14.09)	58.21 (↓ 16.89)
EVA-CLIP ViT-G/14	Blip-2 (FlanT5XL)	4.1B	74.96	71.27 (↓ 3.69)	68.80 (↓ 6.17)	62.01 (↓ 11.88)	59.48 (↓ 15.48)	57.08 (↓ 17.88)
	InstructBLIP (FlanT5XL)	4.1B	76.50	72.07 (↓ 4.43)	69.77 (↓ 6.73)	<u>63.20</u> (↓ 13.30)	63.92 (↓ 12.58)	56.57 (↓ 19.93)

Table 3: Performance Degradation (↓) of VLMs on the VQA task under Wrinkle-like Structural Perturbations Generated from the COCO Dataset. We compare the answer correctness scores (%) evaluated by GPT-4 for baseline methods and the proposed method. Lower values indicate stronger attack performance. Bold numbers denote the best results, and underlined numbers denote the second-best results.

Image Encoder	Models	Params	Clean	Natural Light Attack [14]	Shadow Attack [36]	ITA [21]	Ours (random)	Ours (best)
OpenAI CLIP ViT-L/14	LLaVA-1.5	7B	68.00	68.00 (↓ 0.00)	67.00 (↓ 1.00)	48.00 (↓ 20.00)	55.00 (↓ 13.00)	45.00 (↓ 23.00)
	LLaVA-1.6	7B	64.00	63.00 (↓ 1.00)	64.00 (↓ 0.00)	<u>43.00</u> (↓ 21.00)	47.00 (↓ 17.00)	40.00 (↓ 24.00)
	OpenFlamingo	3B	45.00	39.00 (↓ 6.00)	44.00 (↓ 1.00)	19.00 (↓ 26.00)	20.00 (↓ 25.00)	14.00 (↓ 31.00)
	Blip-2 (FlanT5XL, ViT-L)	3.4B	63.00	58.00 (↓ 5.00)	50.00 (↓ 13.00)	38.00 (↓ 25.00)	<u>36.00</u> (↓ 27.00)	32.00 (↓ 31.00)
EVA-CLIP ViT-G/14	Blip-2 (FlanT5XL)	4.1B	54.00	53.00 (↓ 1.00)	54.00 (↓ 0.00)	33.00 (↓ 21.00)	32.00 (↓ 22.00)	28.00 (↓ 26.00)
	InstructBLIP (FlanT5XL)	4.1B	68.00	64.00 (↓ 4.00)	62.00 (↓ 6.00)	<u>44.00</u> (↓ 24.00)	45.00 (↓ 23.00)	41.00 (↓ 27.00)

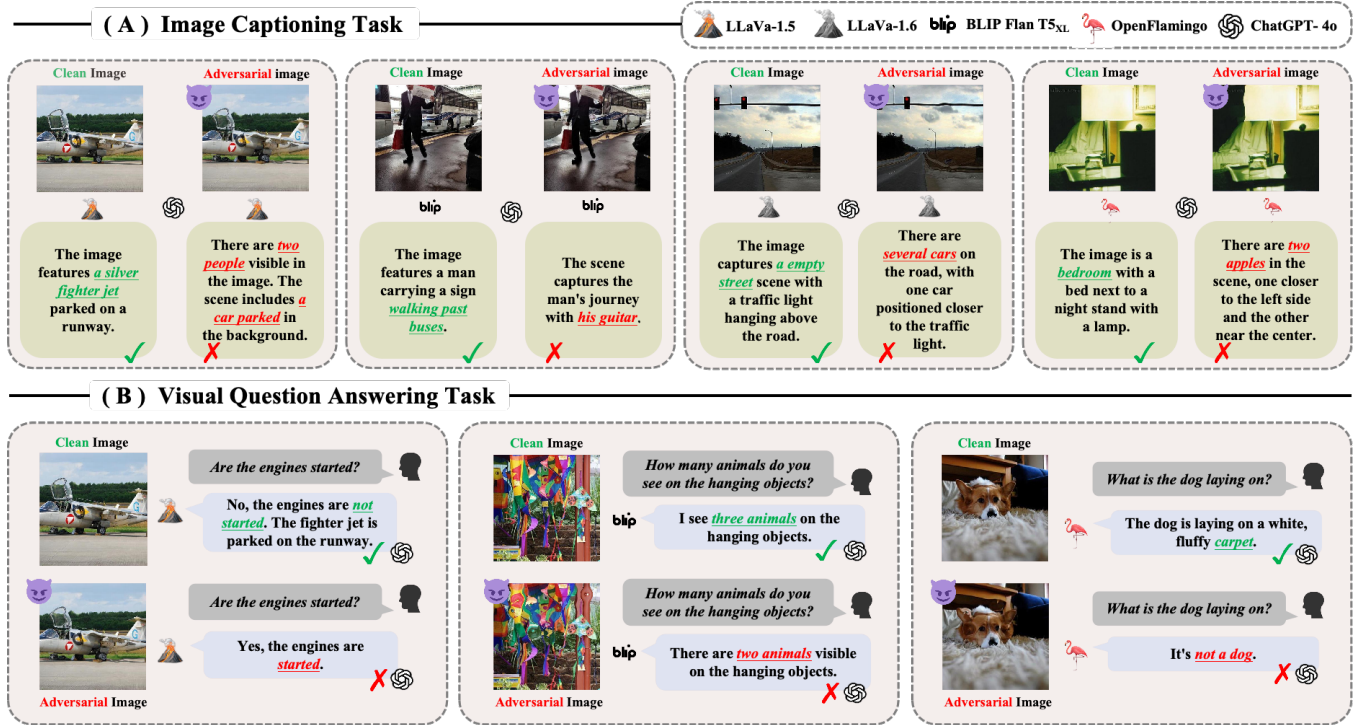


Figure 3: Qualitative Results on Image Captioning and Visual Question-Answering. The figure shows representative outputs for clean and perturbed images, illustrating caption deviations and incorrect answers caused by the proposed perturbation.

5 Ablation Experiments

To better understand the proposed method, we perform several ablation studies on its key design choices and search settings.

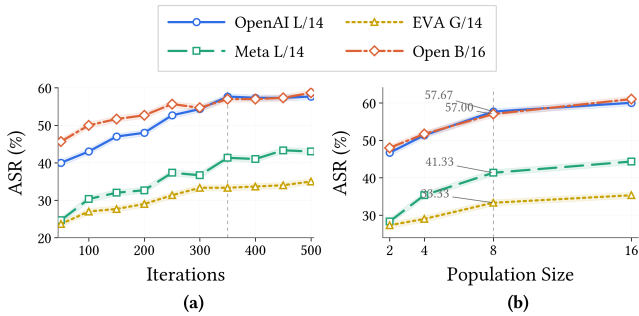


Figure 4: Ablation on Genetic Search Hyperparameters. Attack performance of the proposed wrinkle-like structural perturbation under (a) different numbers of fitness evaluations and (b) different population sizes, showing the trade-off between attack effectiveness and search efficiency across different CLIP models.

Effect of Fitness-Evaluation Budget. We first study the effect of the fitness-evaluation budget on attack performance. As shown in Figure 4 (a), increasing the number of fitness evaluations consistently improves ASR across different CLIP backbones, indicating more effective exploration of the parameter space. However, the gain gradually saturates near 350, suggesting limited additional benefit despite higher computational cost. This result supports the reasonableness of using 350 fitness evaluations in our setting.

Effect of Population Size. We then study the effect of population size on attack effectiveness and search efficiency. As shown in Figure 4 (b), a small population size limits exploration, whereas an overly large population increases per-generation cost without proportional gains. Among the tested settings, a population size of 8 provides the best trade-off between attack effectiveness and efficiency, supporting the rationality of our parameter choice.

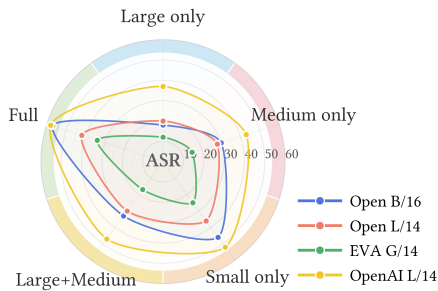


Figure 5: Ablation on multi-scale wrinkle components. ASR (%) under different component combinations is reported, including large only, medium only, small only, large+medium, and full.

Effect of Multi-scale Wrinkle Components. We further analyze the effect of different wrinkle components on attack performance. As shown in Figure 5, the *Full* setting, which combines large-, medium-, and small-scale perturbations, consistently achieves the best or near-best ASR across all models. In contrast, *Large only*, *Medium only*, and *Small only* denote using only the corresponding single-scale component, while *Large+Medium* uses the large- and

medium-scale components without the small-scale one. Among these reduced settings, *Small only* generally outperforms *Large only* and *Medium only*, suggesting that fine-scale perturbations play a more important role in disrupting model perception. However, *Large+Medium* remains inferior to *Full*, further highlighting the importance of the small-scale component. Overall, these results indicate that the proposed attack benefits from multi-scale complementarity rather than any single scale alone.

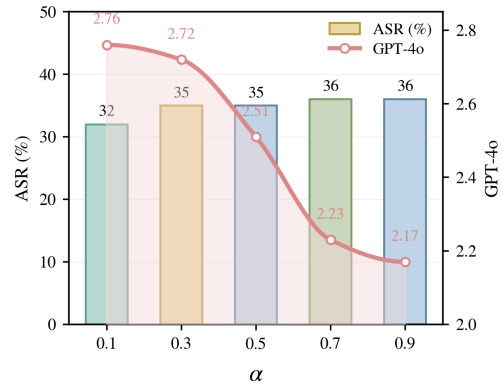


Figure 6: Ablation of the perceptual-similarity weighting coefficient α on EVA-CLIP ViT-G/14.

Effect of the Perceptual-Similarity Weighting Coefficient. We finally study the effect of the perceptual-similarity weighting coefficient α on attack performance and visual quality. As shown in Figure 6, increasing α generally improves ASR but leads to a noticeable decline in the GPT-4o score, indicating reduced visual quality. These results suggest that α governs the trade-off between attack effectiveness and naturalness. Considering both aspects, the choice of $\alpha = 0.3$ is reasonable, as it provides a favorable balance between attack success and visual quality.

6 Conclusion

The robustness of vision-language models under wrinkle-like structural perturbations is systematically evaluated through a parametric attack framework based on non-rigid geometric deformation. Experimental results show consistent performance degradation in zero-shot classification, together with effective transfer to image captioning and visual question answering. Compared with Natural Light, Shadow, and ITA, the proposed method demonstrates stronger attack effectiveness across multiple models, while attention visualizations indicate that the perturbation shifts model focus away from semantically relevant regions. These findings suggest that vision-language models remain vulnerable to structured non-rigid perturbations beyond additive noise.

References

- [1] Jean-Baptiste Alayrac, Jeff Donahue, Pauline Luc, Antoine Miech, Iain Barr, Yana Hasson, Karel Lenc, Arthur Mensch, Katherine Millican, Malcolm Reynolds, et al. 2022. Flamingo: a visual language model for few-shot learning. *Advances in neural information processing systems* 35 (2022), 23716–23736.
- [2] Moustafa Alzantot, Yash Sharma, Supriyo Chakraborty, Huan Zhang, Cho-Jui Hsieh, and Mani B Srivastava. 2019. Genattack: Practical black-box attacks

- with gradient-free optimization. In *Proceedings of the genetic and evolutionary computation conference*. 1111–1119.
- [3] Anish Athalye, Logan Engstrom, Andrew Ilyas, and Kevin Kwok. 2018. Synthesizing robust adversarial examples. In *International conference on machine learning*. PMLR, 284–293.
 - [4] Anas Awadalla, Irena Gao, Josh Gardner, Jack Hessel, Yusuf Hanafy, Wanrong Zhu, Kalyani Marathe, Yonatan Bitton, Samir Gadre, Shiori Sagawa, et al. 2023. Openflamingo: An open-source framework for training large autoregressive vision-language models. *arXiv preprint arXiv:2308.01390* (2023).
 - [5] Ronen Basri and David W Jacobs. 2003. Lambertian reflectance and linear subspaces. *IEEE transactions on pattern analysis and machine intelligence* 25, 2 (2003), 218–233.
 - [6] Igor Buzhinsky, Arseny Nerinovsky, and Stavros Tripakis. 2023. Metrics and methods for robustness evaluation of neural networks with generative models. *Machine Learning* 112, 10 (2023), 3977–4012.
 - [7] Nicholas Carlini and David Wagner. 2017. Towards evaluating the robustness of neural networks. In *2017 IEEE Symposium on Security and Privacy (SP)*. Ieee, 39–57.
 - [8] Mehdi Cherti, Romain Beaumont, Ross Wightman, Mitchell Wortsman, Gabriel Ilharco, Cade Gordon, Christoph Schuhmann, Ludwig Schmidt, and Jenia Jitsev. 2023. Reproducible scaling laws for contrastive language-image learning. In *Proceedings of the IEEE/CVF conference on computer vision and pattern recognition*. 2818–2829.
 - [9] Yung-Sung Chuang, Yang Li, Dong Wang, Ching-Feng Yeh, Kehan Lyu, Ramya Raghavendra, James Glass, Lifei Huang, Jason Weston, Luke Zettlemoyer, et al. 2025. Meta clip 2: A worldwide scaling recipe. *arXiv preprint arXiv:2507.22062* (2025).
 - [10] Xuanming Cui, Alejandro Aparcedo, Young Kyun Jang, and Ser-Nam Lim. 2024. On the robustness of large multimodal models against image adversarial attacks. In *Proceedings of the IEEE/CVF Conference on Computer Vision and Pattern Recognition*. 24625–24634.
 - [11] Wenliang Dai, Junnan Li, Dongxu Li, Anthony Tiong, Junqi Zhao, Weisheng Wang, Boyang Li, Pascale N Fung, and Steven Hoi. 2023. Instructblip: Towards general-purpose vision-language models with instruction tuning. *Advances in neural information processing systems* 36 (2023), 49250–49267.
 - [12] Logan Engstrom, Brandon Tran, Dimitris Tsipras, Ludwig Schmidt, and Aleksander Madry. 2017. A rotation and a translation suffice: Fooling cnns with simple transformations. (2017).
 - [13] John H Holland. 1992. *Adaptation in natural and artificial systems: an introductory analysis with applications to biology, control, and artificial intelligence*. MIT press.
 - [14] Teng-Fang Hsiao, Bo-Lun Huang, Zi-Xiang Ni, Yan-Ting Lin, Hong-Han Shuai, Yung-Hui Li, and Wen-Huang Cheng. 2024. Natural light can also be dangerous: Traffic sign misinterpretation under adversarial natural light attacks. In *Proceedings of the IEEE/CVF Winter Conference on Applications of Computer Vision*. 3915–3924.
 - [15] Max Jaderberg, Karen Simonyan, Andrew Zisserman, et al. 2015. Spatial transformer networks. *Advances in neural information processing systems* 28 (2015).
 - [16] Junnan Li, Dongxu Li, Silvio Savarese, and Steven Hoi. 2023. Blip-2: Bootstrapping language-image pre-training with frozen image encoders and large language models. In *International conference on machine learning*. PMLR, 19730–19742.
 - [17] Junnan Li, Dongxu Li, Caiming Xiong, and Steven Hoi. 2022. Blip: Bootstrapping language-image pre-training for unified vision-language understanding and generation. In *International conference on machine learning*. PMLR, 12888–12900.
 - [18] Tsung-Yi Lin, Michael Maire, Serge Belongie, James Hays, Pietro Perona, Deva Ramanan, Piotr Dollár, and C Lawrence Zitnick. 2014. Microsoft coco: Common objects in context. In *European conference on computer vision*. Springer, 740–755.
 - [19] Haotian Liu, Chunyuan Li, Yuheng Li, and Yong Jae Lee. 2024. Improved baselines with visual instruction tuning. In *Proceedings of the IEEE/CVF conference on computer vision and pattern recognition*. 26296–26306.
 - [20] Haotian Liu, Chunyuan Li, Qingyang Wu, and Yong Jae Lee. 2023. Visual instruction tuning. *Advances in neural information processing systems* 36 (2023), 34892–34916.
 - [21] Hanqing Liu, Shouwei Ruan, Yao Huang, Shiji Zhao, and Xingxing Wei. 2025. When Lighting Deceives: Exposing Vision-Language Models’ Illumination Vulnerability Through Illumination Transformation Attack. In *Proceedings of the IEEE/CVF International Conference on Computer Vision*. 10485–10495.
 - [22] Dong Lu, Zhiqiang Wang, Teng Wang, Weili Guan, Hongchang Gao, and Feng Zheng. 2023. Set-level guidance attack: Boosting adversarial transferability of vision-language pre-training models. In *Proceedings of the IEEE/CVF International Conference on Computer Vision*. 102–111.
 - [23] J. Lu et al. 2024. Unsegment Anything by Simulating Deformation. In *Proceedings of the IEEE/CVF Conference on Computer Vision and Pattern Recognition*.
 - [24] Alec Radford, Jong Wook Kim, Chris Hallacy, Aditya Ramesh, Gabriel Goh, Sandhini Agarwal, Girish Sastry, Amanda Askell, Pamela Mishkin, Jack Clark, et al. 2021. Learning transferable visual models from natural language supervision. In *International conference on machine learning*. PmlR, 8748–8763.
 - [25] Shouwei Ruan, Hanqing Liu, Yao Huang, Xiaoqi Wang, Caixin Kang, Hang Su, Yinpeng Dong, and Xingxing Wei. 2025. Advdreamer unveils: Are vision-language models truly ready for real-world 3d variations?. In *Proceedings of the IEEE/CVF International Conference on Computer Vision*. 7894–7904.
 - [26] Quan Sun, Yuxin Fang, Ledell Wu, Xinlong Wang, and Yue Cao. 2023. Eva-clip: Improved training techniques for clip at scale. *arXiv preprint arXiv:2303.15389* (2023).
 - [27] Aayush Atul Verma, Amir Saeidi, Shamanthak Hegde, Ajay Therala, Fenil Denish Bardoliya, Nagaraju Machavarapu, Shri Ajay Kumar Ravindhiran, Srija Malyala, Agneet Chatterjee, Yezhou Yang, et al. 2024. Evaluating multimodal large language models across distribution shifts and augmentations. In *Proceedings of the IEEE/CVF Conference on Computer Vision and Pattern Recognition*. 5314–5324.
 - [28] Donghua Wang, Wen Yao, Tingsong Jiang, Chao Li, and Xiaoqian Chen. 2023. Rfla: A stealthy reflected light adversarial attack in the physical world. In *Proceedings of the IEEE/CVF international conference on computer vision*. 4455–4465.
 - [29] Zhou Wang, Alan C Bovik, Hamid R Sheikh, and Eero P Simoncelli. 2004. Image quality assessment: from error visibility to structural similarity. *IEEE transactions on image processing* 13, 4 (2004), 600–612.
 - [30] Peng Xie, Yequan Bie, Jianda Mao, Yangqiu Song, Yang Wang, Hao Chen, and Kani Chen. 2025. Chain of Attack: On the Robustness of Vision-Language Models Against Transfer-Based Adversarial Attacks. In *Proceedings of the Computer Vision and Pattern Recognition Conference*. 14679–14689.
 - [31] Hu Xu, Saining Xie, Xiaoqing Ellen Tan, Po-Yao Huang, Russell Howes, Vasu Sharma, Shang-Wen Li, Gargi Ghosh, Luke Zettlemoyer, and Christoph Feichtenhof. 2023. Demystifying clip data. *arXiv preprint arXiv:2309.16671* (2023).
 - [32] Maxime Zanella and Ismail Ben Ayed. 2024. On the test-time zero-shot generalization of vision-language models: Do we really need prompt learning?. In *Proceedings of the IEEE/CVF Conference on Computer Vision and Pattern Recognition*. 23783–23793.
 - [33] Chiyu Zhang, Lu Zhou, Xiaogang Xu, Jiafei Wu, and Zhe Liu. 2025. Adversarial attacks of vision tasks in the past 10 years: A survey. *Comput. Surveys* 58, 2 (2025), 1–42.
 - [34] Jiaming Zhang, Qi Yi, and Jitao Sang. 2022. Towards adversarial attack on vision-language pre-training models. In *Proceedings of the 30th ACM International Conference on Multimedia*. 5005–5013.
 - [35] Richard Zhang, Phillip Isola, Alexei A Efros, Eli Shechtman, and Oliver Wang. 2018. The unreasonable effectiveness of deep features as a perceptual metric. In *Proceedings of the IEEE conference on computer vision and pattern recognition*. 586–595.
 - [36] Yiqi Zhong, Xianming Liu, Deming Zhai, Junjun Jiang, and Xiangyang Ji. 2022. Shadows can be dangerous: Stealthy and effective physical-world adversarial attack by natural phenomenon. In *Proceedings of the IEEE/CVF conference on computer vision and pattern recognition*. 15345–15354.
 - [37] Shuai Zhou, Chi Liu, Dayong Ye, Tianqing Zhu, Wanlei Zhou, and Philip S Yu. 2022. Adversarial attacks and defenses in deep learning: From a perspective of cybersecurity. *Comput. Surveys* 55, 8 (2022), 1–39.